A&A 464, 229–234 (2007)
DOI: 10.1051/0004-6361:20066009

Astronomy & Astrophysics

Compositional dependence of infrared absorption spectra of crystalline silicates

III. Melilite solid solution

H. Chihara[1,2], C. Koike[2], and A. Tsuchiyama[1]

[1] Department of Earth and Space Science, Graduate school of Science, Osaka University, 1-1, Machikaneyama, Toyonaka, Osaka 560-0043, Japan
e-mail: chi@ess.sci.osaka-u.ac.jp
[2] Laboratory of Physics, Kyoto Pharmaceutical University, Misasagi, Yamashina, Kyoto 607-8414, Japan

Received 11 July 2006 / Accepted 13 October 2006

ABSTRACT

The infrared optical properties and absorption spectra of the melilite solid solution series are reported. Melilite is a high-temperature condensate, and is expected to condense during the early phase of the condensation sequence. In this study, samples of the melilite solid solution series were newly synthesized between the aluminium end member (gehlenite) and the magnesium end member (åkermanite) at ~10% intervals in chemical composition, and the infrared absorption spectra of their samples were measured. Variation in the absorption features were detected: such variations include changes in numbers of absorption peaks, peak intensity, peak position, and peak width. The prominent absorption peaks appeared at 10–13 micron, 14, 15, 17, 19, 21, 24, 30, 37 and in the 60 micron region. In particular, the 10 micron feature complex and the 60 micron broad features are very sensitive to chemical composition. For application to and implications for astronomical data, we focused on the 60 micron feature, and carried out a comparison with ISO data of NGC 6302. Our data set will supply the spectroscopic basis for the interpretation of astronomical data accumulated by space and ground based observatories such as ISO, the Spitzer Space Telescope, the AKARI (ASTRO-F) and the Subaru telescope.

Key words. ISM: dust, extinction – ISM: lines and bands – infrared: ISM – circumstellar matter

1. Introduction

An important results obtained with the ISO (Infrared Space Observatory, Kessler et al. 1996) is the discovery of crystalline materials in circumstellar environments of various evolutionary phases of stars (Waters et al. 1996; Waelkens et al. 1996; Whittet et al. 1996; etc.). Particularly, in circumstellar regions of oxygen rich young and evolved stars, the existence of olivine $(Mg_xFe_{1-x})_2SiO_4$ and pyroxene $(Mg_xFe_{1-x})SiO_3$ has been revealed by comparison between observational and experimental studies (Molster et al. 1999; Malfait et al. 1998; Koike et al. 1993; Jäger et al. 1998; etc.). Olivine and pyroxene are expected mineral species based upon equilibrium condensation theory, and their spectroscopic behaviors have been studied extensively in laboratories within the last decade. The dependence of infrared spectra on chemical composition for these mineral species is an important parameter to understand the physical and chemical conditions in the circumstellar environment and also the formation processes of dust grains. Therefore, in our previous series of papers, we examined Mg-Fe pyroxenes (Chihara et al. 2002) and olivines (Koike et al. 2003), and a dependence of their spectra on their chemistry was detected as clear systematic variations of peak shift, peak width and relative intensity ratio. From astronomical observations, it is reported that the chemical composition of circumstellar olivine and pyroxene are extremely Mg rich and the Fe concentration is highly depleted. There are also many mineral species present that are interesting from an astronomical point of view. In many cases, such mineral species occur commonly in meteorites and are major constituents of rock-forming minerals of the Earth's upper mantle. However, for most of these minerals, the infrared optical properties have not yet been reported. In this study, we focused on crystalline melilite. We synthesize members in the series of solid solution that have various Mg-Al ratios, and measure their infrared absorption spectra to obtain information concerning the spectral dependence of this series on chemical composition.

We will briefly discuss the mineralogy of melilite, and its chemistry and crystal structure in Sect. 2. The experimental procedures which include synthesis of the solid solution and characterization of the product materials, and the methods used for the infrared measurements are given in Sect. 3. In Sects. 4 and 5, the results are shown and implications for astrophysics are discussed based on a comparison between laboratory data and ISO observations.

2. Brief mineralogy of the melilite system

Generally, melilite is a silicate mineral with a relatively high equilibrium condensation temperature (1625 K) under typical solar nebular pressures of $\sim 10^{-3}$ atm, and that occurs commonly in CAIs (Ca and Al-rich inclusions) of primitive chondrites. Equilibrium condensation theory predicts that melilite condensed in the early stage of the condensation sequence as a mineral species that includes calcium and aluminium. The chemical formula of a terrestrial sample is represented generally as $(Na, Ca)_2(Mg, Fe^{2+}, Al)(Al, Si)_2O_7$. In CAIs, particularly, Na and Fe^{2+} are highly depleted: this mineral species forms a solid solution between the Al end member,

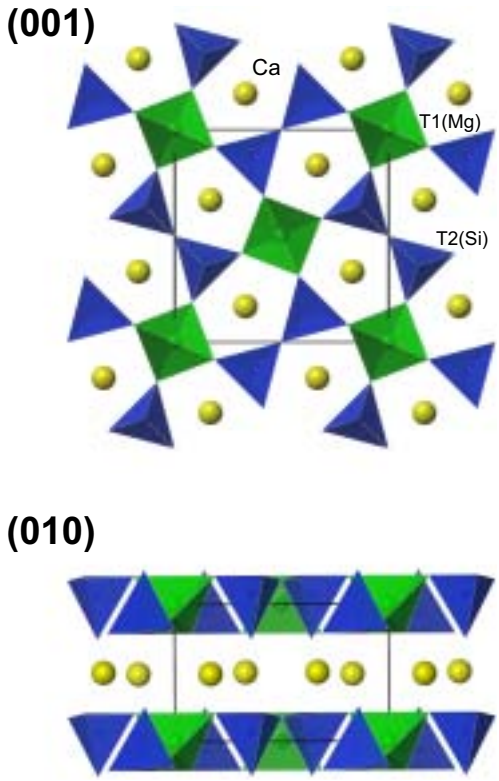

Fig. 1. Melilite (åkermanite) structure projected on the (001) plane and the (010) plane. The unit cell is represented by the central square. In åkermanite, the sites of the Mg and Si ions are ordered in T1 and T2 tetrahedra, respectively. But in gehlenite, the ordering scheme for Al and Si ions is different, that is Al can be located in both of the T1 and T2 tetrahedra, but Si can only be located in T2 tetrahedra (Deer et al. 1992). The plots are made from the data of Kusaka et al. (2001).

gehlenite (Ge:$Ca_2Al_2SiO_7$) and the Mg end member, åkermanite (Åk:$Ca_2MgSi_2O_7$). In this case, the chemical composition of $Åk_X$ is represented as $Ca_2Al_{2(1-x)}Mg_xSi_{1+x}O_7$, $(0 \leq x \leq 1)$. Here we suppose that X is the mole percentage of the åkermanite component ($X = 100x$). The fundamental structure of melilite is based on a tetragonal system, and its space group is classified as $P\bar{4}2_1m$ (D^5_{2d}). A schematic of the melilite (åkermanite) structure projected on the (001) and (010) plane is shown in Fig. 1. In the unit cell of the åkermanite crystal, the site of a Mg atom (or an Al atom for solid solutions and gehlenite) is coordinated as a face centered cubic. These Mg or Al sites are in tetrahedra of oxygen atoms which are shared by adjacent SiO_4 tetrahedra. The linkage between Mg (or Al) and Si tetrahedra forms five-membered rings. Because of this characteristic structure, melilite is sometimes called a "ring" silicate, as opposed to olivine and pyroxene, called "isolated" and "chain" silicates, respectively. The spectral behavior depends on chemical composition and is very interesting and useful in an astronomical context for the identification of observed crystalline features and to trace the path of the condensation sequence when dust grains form in circumstellar regions from their parent gas.

3. Experiment

3.1. Synthesis procedure

To synthesize a sample of the solid solution of crystalline melilite, reagent grade chemical powders of $CaCO_3$, Al_2O_3, MgO and SiO_2 were obtained. From the chemical formula of the melilite solid solution, the mole ratio of these starting materials for $Åk_X$ is represented as $CaCO_3$:Al_2O_3:MgO:SiO_2 = $2:1-x:x:1+x$. Following this ratio, we made mixtures of starting materials. In this study, we prepared 11 samples. The increment in chemical composition between the two end members is ∼10%. The mixtures of starting materials were pressed into pellets 5 mm in diameter and 3 ∼ 4 mm thick. Each pellet weighted approximately 0.1 g.

Heating temperatures were determined from the phase diagram at atmospheric pressure (Osborn & Schairer 1941). Pellets of starting materials were heated at atmospheric pressure at sub solidus (slightly lower by about 10–20 K below the melting point) for approximately 4 days. For $Åk_0$(=Ge_{100}), the duration of heating was shorter than for other materials to avoid damage to the furnace, since the temperature was extremely high, close to 1600 °C. We never melted the starting materials; solid phase reactions were used to synthesize the samples. After heating, the products were quenched in air. The products are polycrystalline aggregations in which the grains grew by sintering.

The chemical compositions were analyzed using an electron probe micro analyser (EPMA:JEOL733) at Osaka University. As a result, we found that the compositions of the product materials are almost consistent with the nominal compositions. Figure 2 shows the result of SEM imaging analysis with back scatter images. The products are uniform and no phase separation was detected. There are some small holes in the polished surface of the product materials (Fig. 2a). In these holes, aggregations of microcrystals are exposed on the inner walls. The shapes of these microcrystals are tetragonal, which reflects the idiomorphic crystalline system of this mineral species. The sizes of the microcrystals ranged up to approximately 10 microns (Fig. 2b). The conditions of the syntheses and the results of our chemical analyses are listed in Table 1.

3.2. Infrared measurements

To prepare the sample pellets for absorption measurements, we used a standard method: after crushing and grinding the products in an agate mortar, the resultant powder had a size of less than 1 μm and was dispersed and embedded in KBr or low density polyethylene for the mid- and far-infrared measurements, respectively. The FT-IR spectrometer (Nicolet Nexus 670) at Kyoto Pharmaceutical University was used to measure the spectra. The measured wavenumber ranges are 7000–400 cm^{-1} (1.5 ∼ 25 μm) for the mid-IR and 650–50 cm^{-1} (15 ∼ 200 μm) for the far-IR measurements. The spectral resolution was 1.0 cm^{-1} for both ranges. Blank KBr and polyethylene pellets which had the same thickness as typical sample pellets were measured as references. Due to instrumental limitations, the data within the range between 7.5 and 120 μm was found to be acceptable. From the absorbance data, the mass absorption coefficients $\kappa(cm^2/g)$ were derived.

4. Results

Figure 3 shows the mass absorption coefficients $\kappa(cm^2/g)$ of the solid solution series versus wavelength in microns. The upper plot is for åkermanite, and the bottom plot is for gehlenite. From the top to the bottom, the concentration of åkermanite decreases in ∼10% increments. Systematic spectral variations depending on chemical composition can be seen, for example, in the number of absorption peaks, the peak intensities, their intensity ratios, peak positions, peak widths, and so on. There are

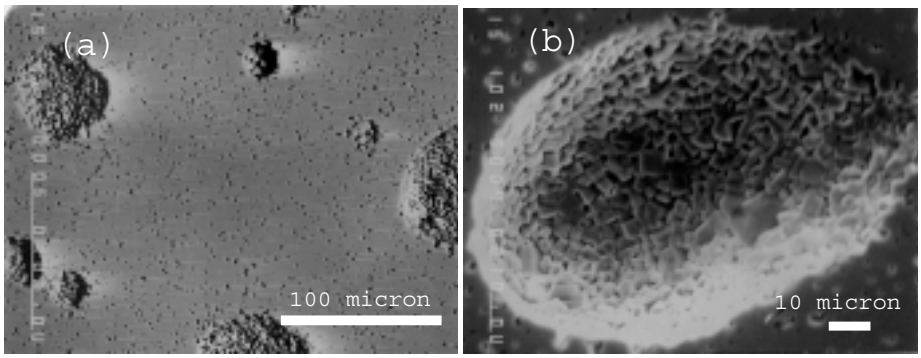

Fig. 2. a) *Left panel* is a SEM with a back scattered image of the polished surface of the $Åk_{50}$ sample. **b)** *Right panel* is a close up image of a hole on the same sample surface. Tetragonal shaped microcrystal aggregations are exposed on the inner wall.

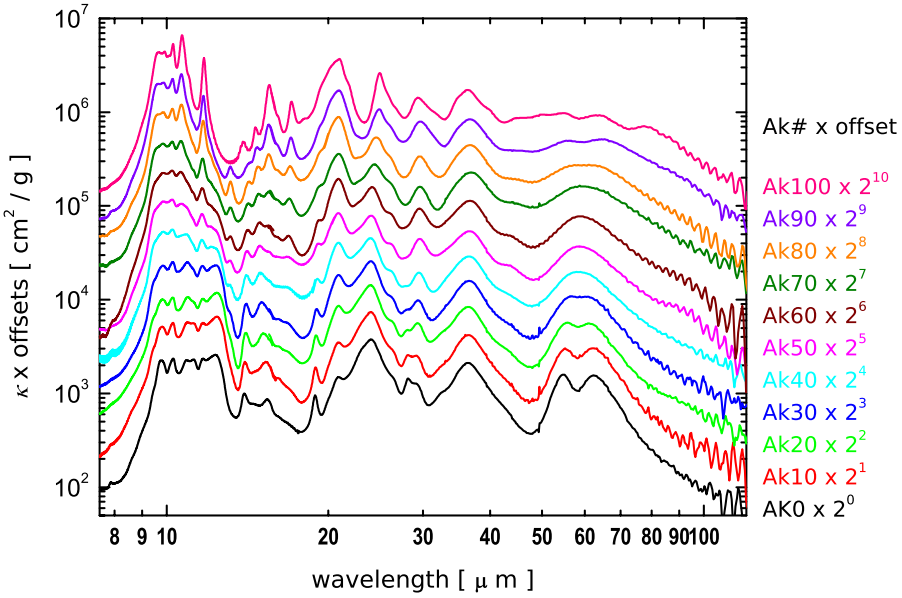

Fig. 3. Mass absorption coefficient $\kappa(\mathrm{cm}^2/\mathrm{g})$ for all samples. The *left panel* is for mid-IR measurement and the *right one* is for far-IR measurement. Numbers on the right side are åkermanite concentration.

Table 1. Synthesis temperature, time and analyzed chemical composition.

Sample name	Temperature °C	Heating duration/h	Åkermanite concentration
$Åk_{100}$	1420	92	Åk100.0
$Åk_{90}$	1400	90	Åk90.4 ± 1.7
$Åk_{80}$	1380	91	Åk77.5 ± 0.8
$Åk_{70}$	1380	91	Åk65.6 ± 2.8
$Åk_{60}$	1380	91	Åk56.8 ± 1.0
$Åk_{50}$	1380	91	Åk46.0 ± 0.8
$Åk_{40}$	1400	90	Åk39.4 ± 0.7
$Åk_{30}$	1420	91	Åk29.6 ± 1.0
$Åk_{20}$	1460	91	Åk16.9 ± 0.3
$Åk_{10}$	1510	91	Åk8.5 ± 0.5
$Åk_{0}$	1560	30	Åk0.2 ± 0.1

approximately 13–15 absorption peaks within the measured infrared region. Although the number of peaks varies depending on the chemistry, the most prominent peaks are located in the 9–13 micron region, and at 14, 15, 17, 19, 21, 24, 30, 37 and 60 microns. The positions of all of the absorption peaks are listed in Table 4. In this work, we used Lorentz fitting to determine peak positions. It is a useful technique to find very small shoulders and broad peaks, particularly in cases where the spectra are very complex. In Table 4, peak positions written in bold face font are shoulders, underlined positions are very broad peaks or plateaus. Values bracketed by parentheses mean that the peaks are extremely small: e.g. too small or broad to find by eye, but that are required to decrease the residues of Lorentz fitting.

In comparison with the spectra of olivine (Koike et al. 2003) and pyroxene (Chihara et al. 2002), the spectral dependency on chemical composition of melilite is very sensitive, particularly in the mid-IR region. For the solid solution close to the aluminium end member (=$Åk_{100}$), there are some extremely sharp and prominent peaks in the 10 micron region (10.3, 10.9 that shifts to 10.7 and 11.7 μm), which are never seen in the spectra of olivine and pyroxene. The intensities of these features increases with increasing åkermanite concentration. In contrast to åkermanite, for the magnesium end member (=$Åk_0$) the shape of the 10 micron feature complex is trapezoidal. This feature is comprised of individual features located at 9.7, 10.3, 10.9, 11.3, 11.7 and 12.4 μm. As the åkermanite concentration increases, the 10.3, 10.7 and 11.7 μm peaks gradually grow and the 12.4 μm peak vanishes. In the region between 13–18 μm, there are four relatively small peaks. Their positions are approximately 14, 14.5, 15.5 and 17 μm. In $Åk_0$, two of these features (14.5 and 16.9 μm features) are very small or only present as a shoulder; however, with increasing åkermanite concentration, these peaks grow gradually and shift slightly, and in $Åk_{100}$, all four peaks became clear.

In the region between 18–30 microns, there are two prominent peaks located at 21 and 24 μm. In the gehlenite composition (=$Åk_0$), the 24 micron peak is larger than the other one. However, with increasing åkermanite concentration, the

Table 2. Peak positions of all samples. Bold fonts mean that the peaks are shoulders or very small. Underlined values are broad peaks or plateaus. Brackets show that the peaks are extremely small, or required only to decrease the residue of Lorentz fitting.

$Åk_0$	$Åk_{10}$	$Åk_{20}$	$Åk_{30}$	$Åk_{40}$	$Åk_{50}$	$Åk_{60}$	$Åk_{70}$	$Åk_{80}$	$Åk_{90}$	$Åk_{100}$
(9.4)	**(9.6)**	**(9.6)**	**(9.4)**	**9.5**	**9.5**	**9.5**	**9.5**	9.5	9.6	9.6
9.8	9.8	9.8	9.8	9.8	(9.8)	(9.8)	(9.8)	(9.9)	(9.9)	(9.9)
										(10.1)
10.3	10.3	10.3	10.3	10.3	(10.2)	(10.2)	10.2	10.2	10.3	10.3
					10.6	10.6	10.6	10.7	10.7	10.7
10.9	10.9	10.9	10.9	10.9	**10.9**					
11.2	11.2	**11.2**	**11.2**			**11.0**	**11.0**	**11.3**	**11.1**	**11.0**
11.7	11.7	11.7	11.7	11.6	11.6	11.7	11.7	11.7	11.7	11.7
				12.1	**12.1**	**12.1**	**(12.2)**	**(12.1)**	**(12.1)**	
12.4	12.4	12.4	12.4	**12.5**	**12.5**	**12.5**		**12.5**		
		13.1	13.2	13.2	13.2	13.2	13.2	13.2	13.2	
										13.9
14.0	14.0	14.1	14.1	14.1	14.1	14.1	14.2	**14.2**	**14.2**	
14.5	14.5									
15.4	15.3	15.2	15.1	15.0	14.9	14.9	14.8	14.8	14.7	14.6
					15.5	**15.5**	15.5	15.5	15.5	15.5
								16.1	**16.2**	**16.1**
16.9	16.7	16.6	**16.6**	**16.7**	16.8	17.0	16.9	17.0	17.0	17.1
										(18.0)
18.9	18.9	18.9	18.9	19.0	19.1	19.1	**19.2**	**(19.3)**	**(20.2)**	**(20.2)**
20.8	20.8	20.9	20.9	20.8	20.8	20.8	20.9	20.9	21.0	21.0
										(21.9)
(22.9)	**(22.9)**					22.8	23.0	22.8		
24.1	24.1	24.0	24.1	24.0	24.1	24.1	24.4	24.6	24.8	24.9
26.2	**26.4**	**26.4**	**26.4**	**26.3**	**26 3**	26.2	**26.2**	**26.1**	**26.3**	**(26.1)**
28.2	28.1	28.0	**28.0**	**27.8**						
29.2	29.2	29.3	29.4	29.5	29.6	29.6	29.6	29.6	29.7	29.4
32.3		(33.0)								
										34.7
36.5	36.5	36.5	36.4	36.3	36.6	36.5	36.7	36.6	36.7	36.4
										39.9
		(42.4)	**43.5**	**43.5**	43.8	43.9	**44.8**	45.0	45.6	45.0
										49.8
54.4	54.8	55.1	55.5					55.7	54.6	55.0
				59.1	59.3	59.5	58.1			
60.0	62.9	62.0	61.8					64.8	66.6	63.7
										79.9

21 micron peak grows gradually, the intensities of the two features become almost equal at intermediate compositions, while at the åkermanite composition, the intensity ratio is reversed. A small peak located at 19 μm in gehlenite vanishes with increasing åkermanite concentration. In addition, there are peaks at 28 and 29 μm in gehlenite, but the former one vanishes with increasing åkermanite concentration, while the latter peak survives in åkermanite.

In the region between 30–50 microns, there is a large feature located at 36.5 μm. The intensities and widths of the 30 and 36 micron features are not very sensitive to chemical composition. On the red wing of the 36 μm peak, a very small shoulder can be seen at approximately 42.5 μm. In gehlenite, this small peak was undetectable, but at intermediate composition ($Åk_{50}$ – $Åk_{60}$) this peak appears as a small shoulder. Its width grows until in the Åk end member, it forms a plateau at around 45–50 μm.

In the Far-IR region from 50 μm to 100 μm, there are some broad and prominent features at around 60 microns. The shapes of these features change depending on chemical composition. For gehlenite, double structured peaks are detected at around 54.4 and 63.0 μm. As the åkermanite concentration increases, these peaks unite to make single feature at intermediate composition ($Åk_{40} \sim Åk_{70}$), and again, split to form very broad triple or quadruple peaks at the åkermanite end member. In olivine and pyroxene, peak locations move to longer wavelength with increasing iron concentration (Jäger et al. 1998; Chihara et al. 2002; Koike et al. 2003). However, in comparison with olivine and pyroxene, the chemical dependency of the spectral features of melilite are not as clear, at least with respect to the

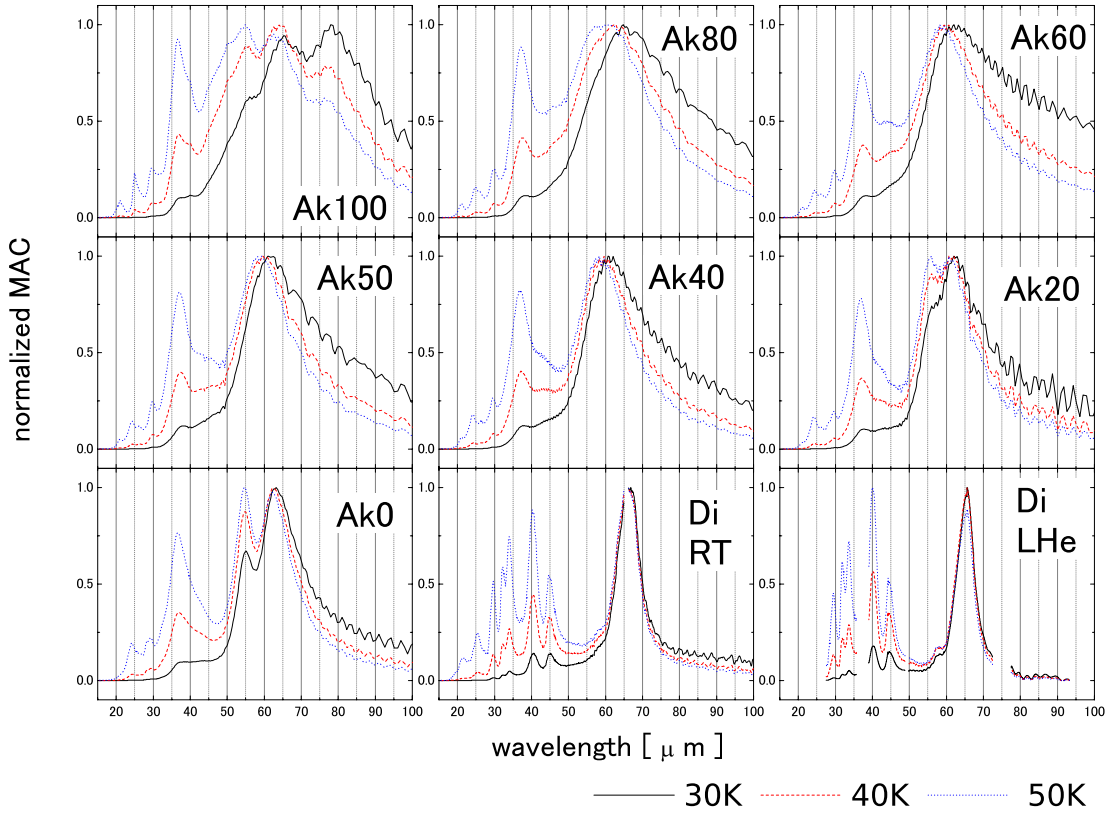

Fig. 4. Normalized mass absorption spectra multiplied by Planck functions at 30, 40, and 50 K. Diopside ($CaMgSi_2O_6$) spectra, which have absorption peak at around 60 μm, obtained at room and LHe temperature (Chihara et al. 2001) are also plotted for comparison.

shift of peak position. Instead, the change of feature shapes due to the change of intensity ratio of adjoining peaks and the behavior of splitting and combining peaks seems to predominate over peak shifting.

5. Application to astrophysics

In this section, we discuss the applications and implications of the laboratory data on melilite for astronomical observations. As mentioned in the previous section, melilite has a prominent, broad feature in the far-IR region at approximately 60 microns. From previous observations by ISO, a broad feature was detected at approximately 63 microns in some oxygen-rich evolved stars, such as AFGL4106, NGC 6302 and HD 161796 (Molster et al. 1999, 2002; etc.) The origin of this feature has been attributed to crystalline materials such as water ice (Molster et al. 1999), diopside $CaMgSi_2O_6$ (Koike et al. 2000; Chihara et al. 2001) and dolomite $(Ca, Mg)CO_3$ (Kemper et al. 2002). Indeed, such candidate materials have broad absorption features at approximately 60 microns that are similar to peaks detected by observation. However, this list includes some minerals that are not reasonable species from the view point of their formation process in space. Therefore, to identify the carrier of this feature, we must consider every possible candidate material that is expected from the condensation sequence and that has a resonance near 60 microns.

Melilite can be considered a candidate carrier for this feature because it has a broad feature at approximately 60 microns. However, since the 60 micron feature of melilite varies its shape depending on its chemistry, to compare the intrinsic shape of this feature, we consider normalized mass absorption coefficients. In Fig. 4, we show the normalized spectra between the end members with compositions every 20% and the 50% samples. Each spectrum is multiplied by the Planck functions at 30, 40 and 50 K, which are indicated by solid, dashed and dotted-dashed lines, respectively. Diopside (Di) spectra, which have an absorption feature at approximately 60 microns, obtained at both room temperature and at liquid helium temperature (Chihara et al. 2001), are also plotted for comparison. The width of the 60 micron peak of melilite is very broad compared to that of diopside. The FWHM of this peak increases with increasing åkermanite concentration and decreasing temperature (Planck function). The peak position changed slightly depending on temperature. The degree of the peak shift is larger for samples with compositions closer to åkermanite, because the width of the peak is broader for higher åkermanite concentration. For both diopside and gehlenite, the change in peak position with variation in the Planck function is not large.

We compare these normalized spectra to astronomical data in Fig. 5. The thick solid line indicates the ISO data for NGC 6302 (Molster et al. 1999). Laboratory data for melilite are superimposed on the spectrum of NGC 6302. The dotted and dashed lines indicate Åk40 at room temperature and diopside measured at LHe temperature multiplied by a Planck function at 30 K. The $Åk_{40}$ spectrum (dotted line) is broader than the 63 micron feature of NGC 6302 and has a different peak position, while for diopside (dashed line), the peak position is closer. However, the width of the diopside peak is too narrow to reproduce the observed 63 micron feature. Here, we try to produce spectra of mixtures of $Åk_{40}$ and diopside using the following formula,

$$F_{\rm mix} = \sum_{i=1}^{2} m_i \kappa_i B(T, \lambda), \qquad (1)$$

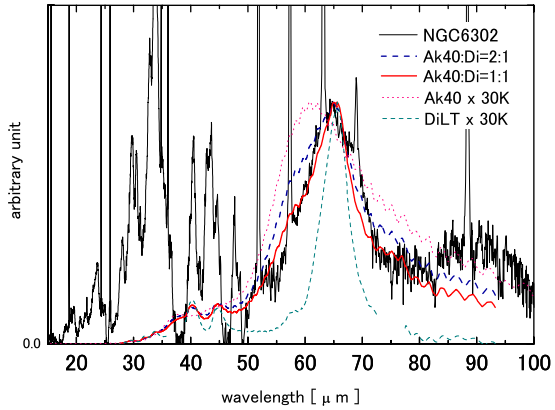

Fig. 5. Comparison between NGC6302 observed by ISO and laboratory spectra.

m_i, κ_i are the mass ratio and mass absorption coefficients for the ith dust component. The Planck function $B(T, \lambda)$ at 30 K is adopted for this comparison. The first trial is a mixture of Åk_{40} and Di at a ratio of two to one (thick dashed line). The peak position of the 60 micron feature is almost consistent with the observed spectrum of NGC 6302. However, the width of this feature is broader than that of the observed one. The next trial is a mixture of Åk_{40} and Di with ratio of one to one (thick line). In this spectrum, both peak position and width seem consistent with the 63 micron feature observed by ISO. The positions of other peaks do not contradict the observed spectrum, because at temperatures as low as 30 K, peaks located at shorter wavelengths are small. From this rather rough comparison, we cannot conlude that melilite is the only carrier of the unidentified 60 micron emission feature. However, we can reproduce the observed spectrum by using a mixture of Åk_{40} and low-temperature diopside with a 1:1 ratio. Since melilite does not contradict the condensation sequence and its chemical composition does not contradict solar abundances, we can propose that melilite should be considered as a new candidate material of cosmic dust components.

6. Summary

This work is summarized as follows:

1. Samples of the solid solution series of melilite were synthesized in the laboratory and measurements of their infrared absorption spectra were carried out. The infrared spectral data set can be used for the interpretation of astronomical data accumulated by satellite missions such as ISO, the Spitzer Space Telescope and the AKARI(ASTRO-F) which has just been launched, as well as other ground based observations.
2. Systematic spectral variations dependent on chemical composition were clearly detected in the number of absorption peaks, peak intensity, peak position and peak width.
3. Melilite has a broad and prominent feature located near 60 microns. The spectral variation of this feature is very sensitive to chemical composition. The spectrum of Åk_{40} and diopside with a mass ratio of 1:1 multiplied by the Planck function at 30 K can reproduce the 63 micron unidentified emission feature observed by ISO in some oxygen rich AGB stars.
4. We propose that the melilite group minerals should be considered as a new component of cirmumstellar dust material. Melilite is consistent with both the equilibrium condensation sequence and solar abundances.

Acknowledgements. We thank to Dr. J. Nuth, the referee, for the valuable comments. We also thank Prof. Dr. L.B.F.M. Waters, Dr. R. Dijkstra, Dr. C. Kemper and for their valuable discussions and comments.
This study was supported by the Ministry of Education, Culture, Sports, Science and Technology of Japan, Grant-in-Aid for Scientific Research on Priority Areas “Development of Extra-solar Planetary Science”.

References

Chihara, H., Koike, C., & Tsuchiyama, A. 2001, PASJ, 53, 243
Chihara, H., Koike, C., Tsuchiyama, A., et al. 2002, A&A, 391, 267
Deer, W. A., Howie, R. A., & Zussman, J. 1992, An introduction to the rock-forming minerals, 2nd edn. (Harlow, England: Pearson Education)
Jäger, C., Molster, F. J., Dorschner, J., et al. 1998, A&A, 339, 904
Kemper, F., Jäeger, C., Waters, L. B. F. M., et al. 2002, Nature, 415, 295
Kessler, M. F., Steinz, J. A., Anderegg, M. E., et al. 1996, A&A, 315, L27
Koike, C., Shibai, H., & Tsuchiyama, A. 1998, MNRAS, 264, 654
Koike, C., Tsuchiyama, A., Shibai, H., et al. 2000, A&A, 363, 1115
Koike, C., Chihara, H., Tsuchiyama, A., et al. 2003, A&A, 399, 1101
Kusaka, K., Hagiya, K., Ohmasa, M., et al. 2001, Phys. & Chem. Min., 28, 150
Malfait, K., Waelkens, C., Bowman, J., et al. 1999, A&A, 345, 181
Molster, F. J., Waters, L. B. F. M., Trams, N. R., et al. 1999, A&A, 350, 163
Molster, F. J., Lim, T. L., Sylvester, R. J., et al. 2001, A&A, 371, 165
Molster, F. J., Waters, L. B. F. M., Tielens, A. G. G. M., et al. 2002, A&A, 382, 241
Osborn, E. F., & Schairer, J. F. 1941, Am. J. Sci., 239, 715
Waelkens, C., Waters, L. B. F. M., De Graauw, M. S., et al. 1996, A&A, 315, L245
Waters, L. B. F. M., Molster, F. J., de Jong, T., et al. 1996, A&A, 315, L361
Whittet, D. C. B., Schutte, W. A., Tielens, A. G. G. M., et al. 1996, A&A, 315, L357